Fundamentals of Melt Atomization, Spray Forming and Deposition

Klaus Bauckhage

Universität Bremen, Institut für Werkstofftechnik
Badgasteiner Straße 3, 28359 Bremen
vt@iwt.uni-bremen.de

The main unit operations of the spray forming process will be described in detail. These are the twin fluid gas atomization of the melt, the mass-, momentum- and enthalpy-transport of the melt particles within the multiphase flow of the spray cone, as well as the deposition, compaction and solidification of the melt particles (together with facultatively added powder particles) within the mixing layer of the deposit. These unit operations are not only consecutive but also conditional steps of the entire spray forming process on the way to generate materials with new and high sophisticated properties. The purpose of our investigations was to understand and describe the atomization process as a base for modelling (and control) of the overall disintegration process and to derive strategies and possibilities for directly influencing the resulting spray properties (and in consequence the material properties of the deposit) of the atomization process. In correspondence with experiments the numerical simulation of the gas flow situation in the vicinity of the individual gas nozzles and their common influence on the melt jet perturbation led to improved atomizer design and thereby higher efficiency of the disintegration process (smaller droplets, lower span and reduced gas consumption).

1. Introduction

Spray forming denotes the fabrication of metallic or ceramic materials in the form of billets, plates, sheets or tubes by melt atomization and spray deposition onto a substrate. Since spray forming is in competition with established metal forming technologies like casting and forging this new technology has to offer several advantages concerning the material properties of its products, such as the absence of macro-segregation, microstructural refinement including fine equiaxed grains, uniformly distributed and extremely fine precipitants and modified primary and/or secondary phases at the grain boundaries, low micro segregations and chemical homogeneity over the entire volume of the pre-product. There also exist some relationships to the metal coating technology of thermal spraying, especially to the high alloying flexibility by adding fine metal powders during the generation of the metal coat – here the generation of metal matrix composites.

Reviewing the evolution of this new technology, one has to acknowledge A.R.E Singer´s pioneering work in the 1970s [1-2], and the introduction of the spray forming process, well known as the Osprey process as a new industrial production route of high sophisticated ma-

terials by his group in the 80s [3-4]. Since 1994 the interdisciplinary collaborative research centre *372 "spray compaction"* of the Deutsche Forschungsgemeinschaft is engaged in basic research works and developments covering this field [5].

Asking for the context of spray forming with *liquid atomization and spray systems* one has to draw the attention to the main unit operations of this integrative process:

- gas atomization or centrifugal atomization of liquid melts of metals, alloys or ceramics
- multiphase flows directing the spray onto a substrate/deposit
- rapid cooling of the melt droplets during this transport
- deposition, compacting and solidification of the melt droplets at the deposit
- generating new compact preforms with advanced material properties.

Furthermore to the *ICLASS-community* it seems worth mentioning that most of the relevant material parameters, governing the disintegration process of the liquid – such as surface tension, density and viscosity – remain on a very different level during the entire spray forming process. Compared with those properties of the well known water atomization, Table 1 gives an impression of these differences.

Table 1: Properties of different fluids

Material	Tliq	T	ρ(T)	η(T)	σ(T)	σ(T) / σH2O
[-]	[°C]	[°C]	[kg/m³]	[mNs/m²)]	[mN/m]	[-]
water						
H2O	0	15	999,1	1,14	74	1
pure metals						
Sn	232	382	6920	1,61	550	7,4
Pb	327	477	10500	1,87	440	5,9
Al	660	810	2340	1,23	850	11,5
Cu	1083	1233	7910	3,20	1300	17,6
Fe	1536	1686	6890	3,64	1800	24,3
alloys						
AlCu4SiMg	650	800	2420	1,45	800	10,8
CuNi2,4Si0,6	1055	1205	7920	3,40	1250	16,9
CuSn6	1050	1200	7840	3,35	1200	16,2
CuSn13,5	985	1135	7755	3,60	1100	14,9

T = temperature; ρ = density; η = viscosity; σ = surface tension; σ_{H2O} = surface tension of water

Provided that the disintegration process (as in our case) is caused by gas atomization, a rapid convective heat extraction takes most of the overheat and partially the latent heat from the particles before they impact on the substrate/deposit. If on the other hand atomization is caused by centrifugal forces in a diluted gas atmosphere, mainly radiation overtakes this heat extraction. In any case, the spray consolidates and solidifies completely on impingement with the substrate, generating there a dense material (pre-product) of advanced metallurgical characteristics. Within the deposit (and in contact with a non-isolating substrate) additional heat conduction leads to a limitation of grain growth and/or to changes of the crystalline phases.

After melting the metallic (ceramic) material and overheating it to a pre-established degree, the melt is delivered under free fall conditions to the atomization zone, see Fig. 1. There the high velocity difference between the melt stream and the impinging high speed gas jets of more than 200 m/s attains an effective disintegration and leads to a wide size distribution of droplets (1 to 300 µm in diameter). This means that their individual surface area differs from each other by a factor of up to 10^4, their mass by a factor of up to 10^7, which explains the differences of droplet accelerations (and velocities) as well as the great variety of release of thermal energy to the gas during their flight to the substrate and also the differences of momentum during droplet impact. These particles – consisting of (liquid) melt droplets, already solid particles and particles that are partially solid – consolidate and solidify completely on impingement with the substrate.

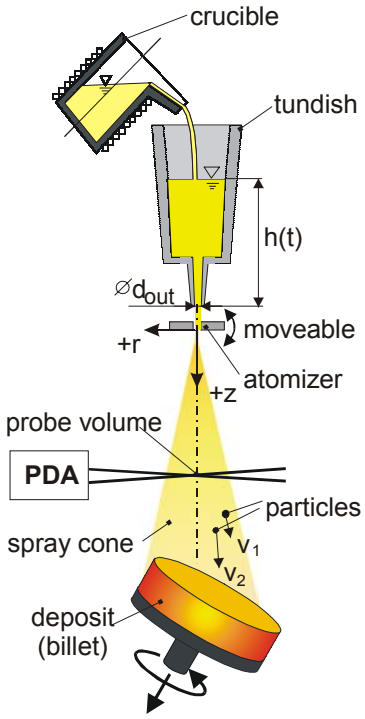

Fig. 1: Sketch of the process and its main devices

The process and its main devices have been sketched in Fig. 1, showing

- the melting device (crucible),
- the tundish,
- the atomizer,
- the spray cone and
- the substrate/deposit.

In the atomization stage the mass flux distribution and enthalpy density distribution in the spray are determined, resulting from the different sizes of droplets and particles and their short thermal histories during their flight within the spray cone from the atomization zone to the impingement onto the deposit surface. The purpose of our investigations was to understand and describe the atomization process as a base for modelling (and control) of the over-

all disintegration process and to derive strategies and possibilities for directly influencing the resulting spray properties (and in consequence the material properties of the deposit) of the atomization process.

2. The Atomization Process

For the melt disintegration two types of twin fluid (gas) atomizers are used, the close coupled (CCA) and the free fall atomizer (FFA) as sketched in Fig. 2. The design of both atomizers is composed of concentric rings (around the central melt stream) containing numbers of identical discrete gas nozzles which eject the gas jets for melt disintegration. While the CCA produces finer particles and allows a lower mass flow ratio of gas to melt (GMR), the FFA is mostly used as a scanning device, thus generating a wider spread and a more uniform mass distribution of the spray. Since the FFA has as main advantage a strong robustness regarding freeze up, this explains its more common use. We confine the following to the free fall atomizer type.

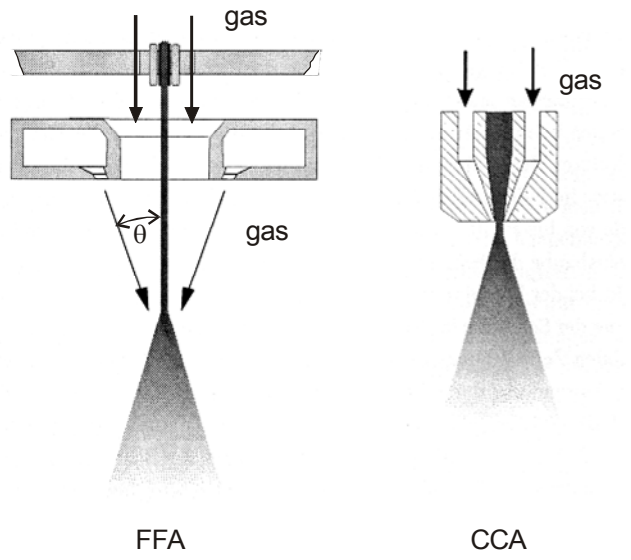

Fig. 2: Twin fluid atomizers for melt disintegration: free fall (FFA) and close couple (CCA)

The twin fluid atomization process of "normal" fluids can be divided into five subsequent stages. This has been adapted also to liquids like metal and ceramic melts. The first three stages can be described by the classical model of Dombrowski and Johns [6].

1st stage : initialisation and growth of perturbation
2nd stage: break up in ligaments
3rd stage: break up of ligaments in droplets.

More recent results recommend the addition of two further stages to this model, Klar and Fresko [7]

4th stage: successive (secondary) break up of larger into smaller droplets
5th stage: collisions and coalescence of droplets in dense flows.

After outlining in the following the flow-conditions of the atomizing gas, the stage of initialisation and growth of surface perturbations of the melt stream until primary break up will be described.

2.1. Gas Flow

In the FFA-configuration the upper primary gas nozzles have to prevent recirculation gas flows in the vicinity of the melt outlet. The atomization gas is delivered by the lower secondary nozzles, which are operated at much higher gas pressures and therefore mass flow rates than the primary nozzles. The emerging melt jet flows due to gravity from the outlet orifice into the atomization region, which is located well below the atomizer. The gas flow of the discrete jet arrangement in the nozzle vicinity, as been described in [8], interacts and forms a common coaxial gas jet, Fig. 3, which finally leads to a parallel flow situation of gas and melt jet. Here disintegration of the melt jet takes place, mainly initialised by shear flow instabilities of the gas liquid interface.

Regarding this gas atomization process, the relevant gas mass flow rates (due to the production rates of tons per hour) are also in the range of a gas consumption of tons of inert gas per hour. So the costs and the efficiency of the disintegration (governed by the atomization gas) have to be focused on. The latter is influenced by the contour of the gas nozzles, the geometry of their arrangement and the process conditions. This explains, why recent developments lead to gas nozzle designs, following more or less the ideal *Laval*-contour, prescribed by the pressure ratio of stagnation pressure p_0 (prior to the nozzle) to ambient pressure p_u (behind the nozzle in the spray chamber), see Fig. 4, [9 -11].

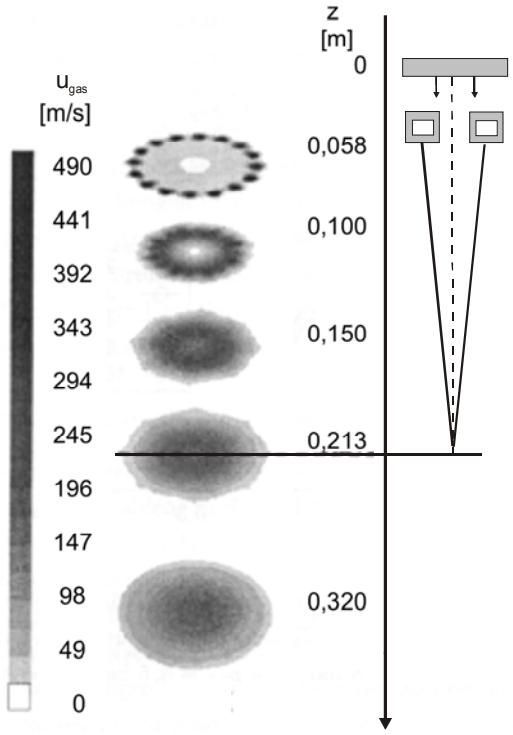

Fig. 3: The gas flow of the discrete jet arrangement in the nozzle vicinity forming a common coaxial gas jet and finally leading to a parallel flow situation

But since the pressure p_0 has also to be used for process control, in most applications it cannot be held constant. Thus the stagnation pressure should exceed the critical value for the necessary (*Laval*-) ratio definitely, adding in consequence the term Δp for atomization gas pressure control:

$$p_0 = p_u \{ 1 + (\kappa - 1) / 2 \, Ma_A^2 \} \exp. (\kappa / \kappa - 1) + \Delta p \qquad (1)$$

with κ being the exponent of isentropic expansion and Ma_A being the exit *Mach*-number, [10].

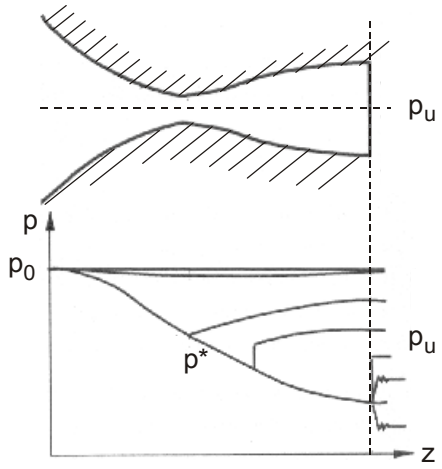

Fig. 4: Ideal *Laval*-contour and process conditions for over/under-expanded gas jets, prescribed by the pressure p_0 (prior to the nozzle) and the ambient pressure p_u (behind the nozzle)

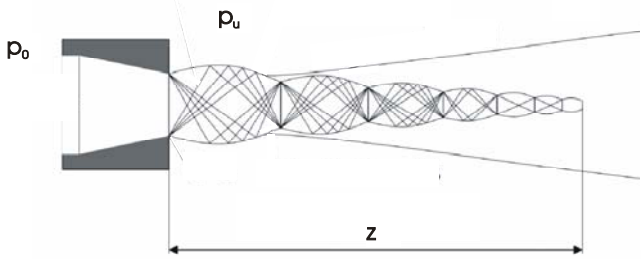

Fig. 5: Sketch of an under-expanded gas jet

For nitrogen and an exit *Mach*-number of 1 the ratio of p_0 / p_u (without Δp) should exceed the value of 1.89. Meeting this condition leads to an under-expanded gas jet, Fig. 5, which for practicable dimensionless distances z/d (z from the nozzle exit) ranges energetically near the ideal-expanded one, Fig. 6 and 7, and which allows to use a simplified convergent/divergent nozzle-contour instead of the smooth ideal *Laval*-contour (that has to be machined with higher effort).

For the over-, ideal- and under-expanded gas jets the correlations between their geometry and their expansion pattern as well as between their centreline gas velocities and the nozzle-distances are given in Fig. 7. The main message from this Figure is, that for growing distances z from the nozzle exit (with d being the nozzle diameter at the *Laval*-cross-section) and relevant values of $z/d > 15$, the centreline-velocity of the under-expanded gas jet ranges

closer to that of the ideal-expanded one than the over-expanded gas jet, while the ideal-expanded gas jet is contributing most of the kinetic energy to the disintegration process of the melt stream.

After optimizing the inclination angle θ (see Fig. 2) of the individual gas nozzles with reference to the melt stream the question arises, how many nozzles and which nozzle diameters are necessary for a given gas mass flow. This generally can be answered already from Fig. 3 and 7: Most of the kinetic energy of the single gas jet has to be brought to that downstream-position where high efforts in melt perturbation can be achieved. In other words: at that position one needs high centreline gas velocities. Regarding the typical long distances of the FFA, this means, one has to reduce the numbers of nozzles in order to raise d and to receive larger distances z, thus high centreline gas velocities can be achieved further downstream. This has been confirmed by atomization measurements, as can be seen from Fig. 8 and 9, [10].

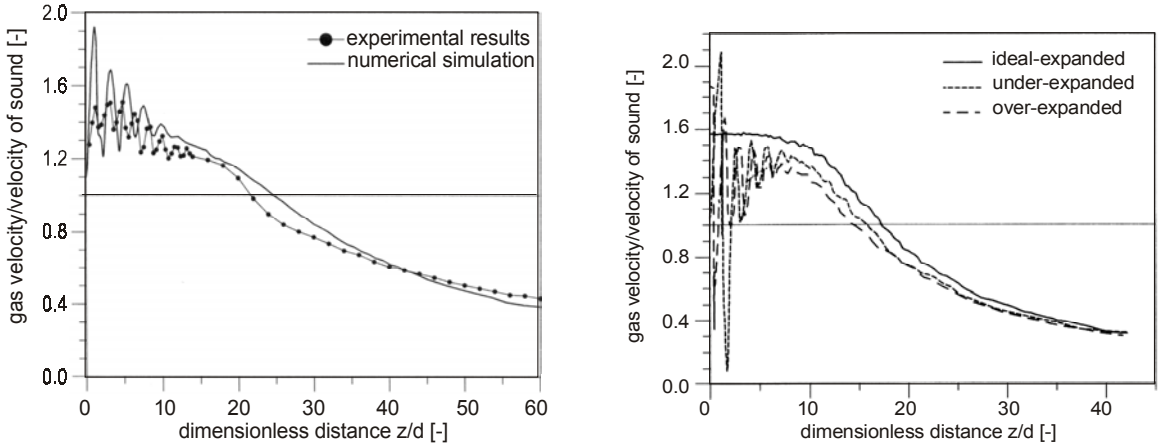

Fig. 6 and 7: Dimensionless: centre-line gas velocity versus distance from the nozzles; (6) measurements and computational results for an under-expanded jet (7) computational results

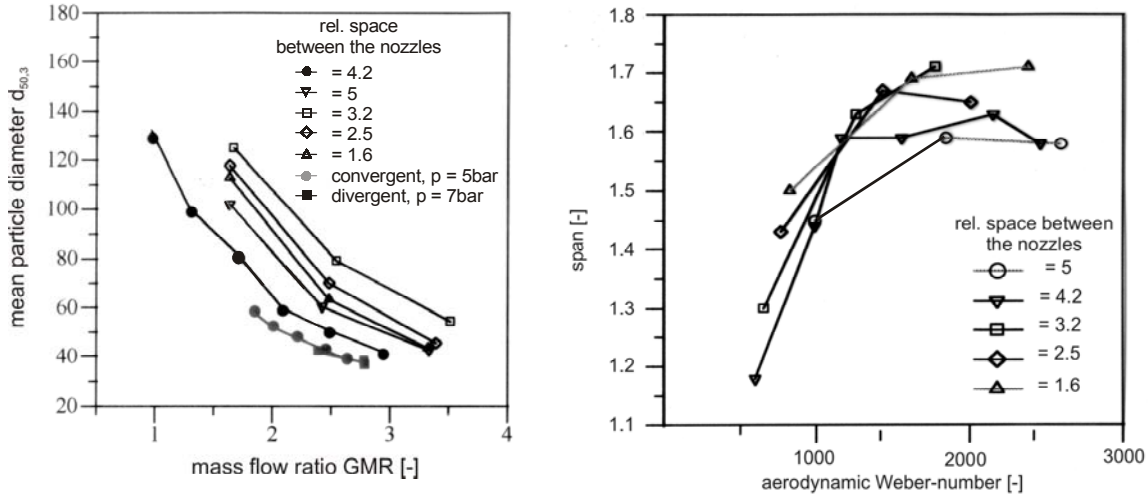

Fig. 8 and 9: Experimental results of median particle diameters versus GMR and of span versus aerodynamic *Weber*-numbers for variation of nozzle-type, -distances and -diameters d

The mass median diameter $d_{50,3}$ is given versus gas to melt mass flow ratio (GMR). The droplet diameter after atomization by different nozzle configurations decreases with increasing GMR and relative distance between the nozzles. The results have been received by the augmentation of the nozzle diameter d and the lowering of the nozzle number N, holding constant the common nozzle exit area ($N \pi d^2/4$ for a given and unchanged GMR). Also the span (i.e. the width of the particle size distribution) can be reduced in the applied *Weber*-number region by increasing distance between the nozzles, which is assumed to depend on the recirculation free gas entrainment in the vicinity of the atomization zone.

If (for constant mass flow conditions) the gas stream is heated up (for instance, to temperatures of about 1070 K) the centreline gas velocity increases significantly. This can be seen from Fig. 10 from [9 and 11], confirming the experimental results, which show that the velocity difference between gas and melt influences the disintegration process and that higher gas temperatures (and therefore higher gas velocities) reduce the size distribution of the melt particles. But this effect is limited, as can be seen from the following theoretical perturbation studies, which show that the growth rate values of the perturbation waves in principle are governed by the lower mode numbers.

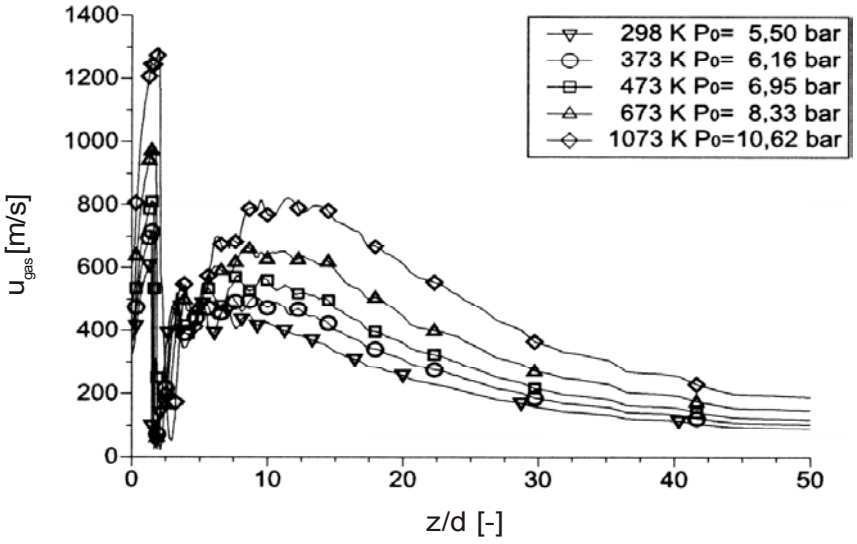

Fig. 10: Centre-line gas velocity versus dimensionless distance from the nozzle for higher gas temperatures

2.2. Melt Disintegration

In order to directly compare results from different experiments and materials it is helpful either to operate at identical parameters and/or to use dimensionless correlations. For twin fluid gas atomization relevant parameters are the aerodynamic *Weber*-number and the liquid *Reynolds*-number:

$$We = (\rho_{gas} \ \Delta u^2 \ d_{melt\text{-}jet}) / \sigma \qquad (2)$$

$$Re = (\rho_{melt} \ u_{melt} \ d_{melt\text{-}jet}) / \mu_{melt} \qquad (3)$$

with ρ_{gas} and ρ_{melt} being the gas and melt density, Δu the velocity difference between gas u_{gas} and melt u_{melt} and with σ and μ_{melt} as surface tension and viscosity and $d_{melt\text{-}jet}$ being the diameter of the melt jet.

Using the phenomenological classification from [6 and 7], the relevant disintegration may be described via fiber-type ligaments in the range 100 < We < 500. For high velocity differences between gas and melt, in this mode the driving forces of the jet break up are aerodynamic forces only. Special care has to be taken using values of the gas velocity in equation (2). Since for the FFA there exist quite long distances between the gas nozzle exits and the atomization region with varying atomization gas velocities, one has to focus on the centreline gas velocity of each gas jet, with reference to Fig. 7, at those distances z, where disintegration takes place, i.e. at that geometrical point, where the single atomization gas jets interact on the centreline of the melt jet.

The range of the *Weber*-number for a typical spray forming process of, for instance tin or steel melt spraying is 100 < We < 400. The influence of the local flow structure inside the melt jet on the disintegration process is that of the turbulent regime, for 10^4 < Re 2 10^4 (which are typical values) and for a stagnant gas atmosphere the melt jet has a more or less smooth surface. With increasing atomization gas pressures (1 bar < p_o < 4.5 bar) the break up length (defined as the length of the continuous liquid jet before break up [12 and 13]) decreases, as given in Fig. 11.

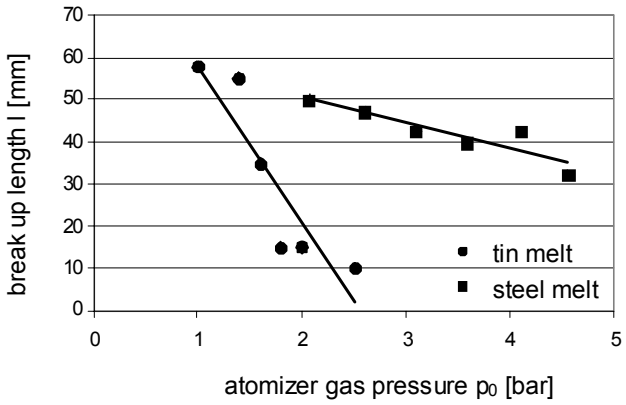

Fig. 11: Decrease of break up length with increasing gas pressure for tin and steel melts

As described in detail in [12], the wave growth of surface perturbations has been studied not only experimentally, but also by stability analysis. Starting from the linearised *Navier-Stokes* equations for both phases (gas and melt) an algebraic solution has been derived, the type and complexity of which depends on the simplifications which have been made. Considering the instability process of the viscous liquid jet discharging from the round melt outlet of diameter $d_{melt\text{-}jet}$ into an infinitely large inviscid gas phase, the liquid jet moves at an overall constant velocity u_{melt}. The velocity of the gas phase u_{gas} has the same direction but is much higher. Both phases are assumed to be incompressible, gravitational forces are neglected. The equation system governing the liquid motion consists of the conservation equations for mass and momentum. For proper linearisation one has to assume that the perturba-

tions are small compared to their mean values: the surface perturbations are small compared with the melt jet diameter and the melt mean velocity is much higher than the perturbation velocity. A further condition is that the pressure in both phases on either side of the interface is identical.

While the 3-D characteristics of the surface perturbations are expressed in terms of the mode n, which is related to the angle of circumference (with principle characteristics of the different instability modes shown in Fig. 12 from [12]), the instability process can also be described by the wave growth ω_{re} after Fig. 13, assuming that the wavelength with the fastest wave growth will dominate the overall disintegration process and that this wavelength differs for different metal melts due to the specific material properties: here mainly the surface tension. The wave growth rate is decreasing with increasing surface tension and hence with increasing wave length.

The first result from these studies is already well known: metallic melts have much lower growth rate values compared with aqueous liquids and therefore need much higher energies (higher velocity differences Δu) than water-based liquids to be disintegrated in the same mode. The second result is that the change of viscosity does not have a significant effect, even though it may result in a more turbulent motion at the outlet, as one can see from the Reynolds-numbers. For much higher relative velocities the importance of higher modes is becoming obvious. The maximum growth rate for the symmetric mode n = 0 is the largest, but the asymmetric mode n =1 is almost of the same order followed by the higher modes, as can be seen from Fig. 14

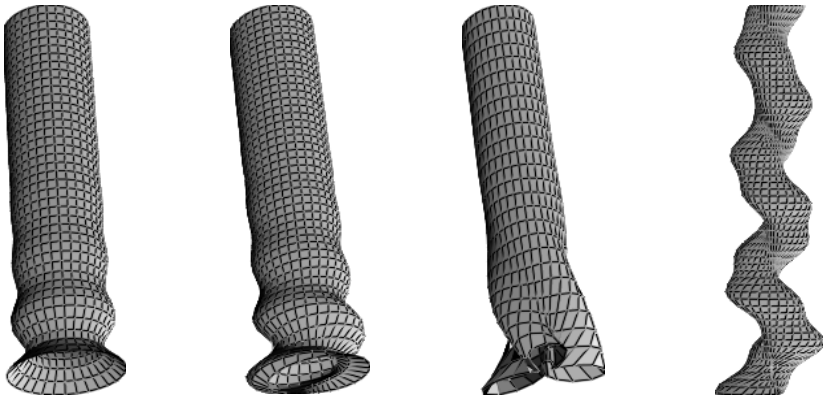

Fig. 12: Growing 3-D-characteristics of surface perturbations with increasing mode n

Summarising the relevant results from chapters 2.1 and 2.2, it could be confirmed that the optimisation of the atomizer design lead either to a reduction of mean spray particle size (for constant gas to melt mass flow ratios, GMR) or to a reduction of gas consumption (for an unchanged particle size distribution). The steps of optimisation are the use of

- convergent divergent gas nozzle contours
- reduced nozzle numbers N and enlarged nozzle diameters d for a given GMR
- a pressure ratio of $p_0 / p_u > 1.9$.

It could not yet been derived a general correlation between gas flow conditions and melt stream perturbation (and break up) and spray droplet size distribution, though this is the main parameter for the mass-, momentum- and enthalpy- transport from the spray cone to the substrate/deposit and is determining the generation of improved material properties.

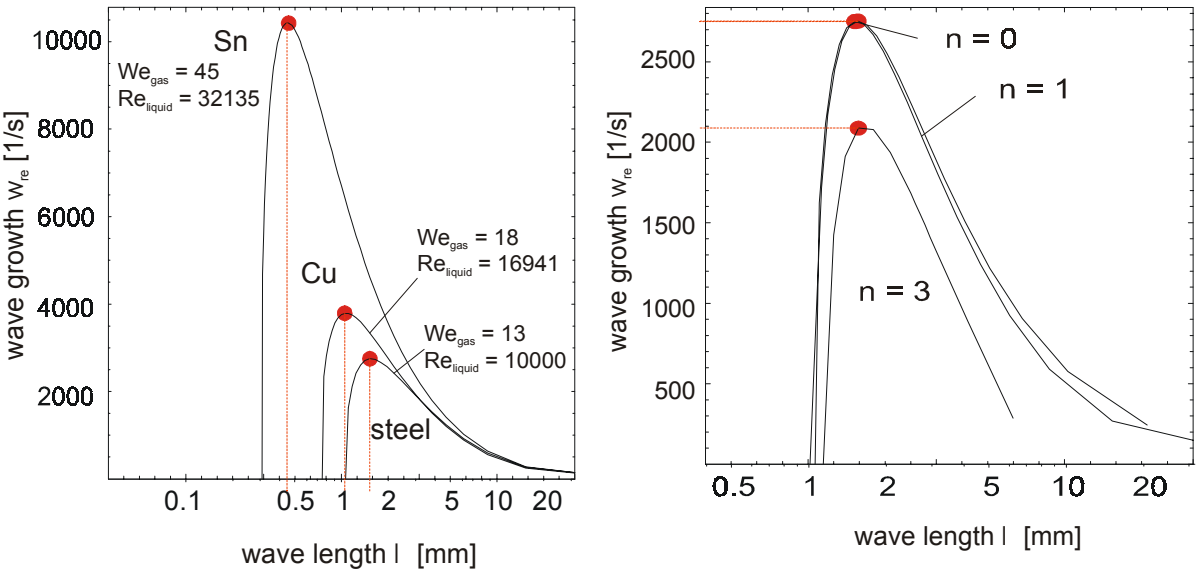

Fig. 13 and 14: Wave growth versus wave length for different materials and modes n

3. Mass-, Momentum- and Enthalpy-Transport

As can be seen already from the simulation results of Fig. 3 and as discussed in detail by [13] the spray cone can be divided in three regions: **a)** the near-nozzle field, **b)** the core area and **c)** the far field. Reducing the discussion to the pure gas flow, the near-nozzle field is characterised by supersonic and further downstream by sonic gas jets from the individual gas nozzles. For short distances behind the nozzle exits several compression shocks may occur (as described in chapter 2.1 by Fig. 5). The core area is located around the geometric point of atomization, while the gas jets merge together and the common overall gas velocity increases until its maximum is reached (at distances of about 150 mm downstream from the atomization gas nozzles). Further downstream, within the far field, the common gas stream forms a single free jet, with its typical axial and radial behaviour and self similar velocity profiles, the strength of which mainly depends on the gas mass flow (due to the gas pressure) [8,9,10,14,15].

This single-phase gas flow is changing dramatically when starting the melt flow and the atomization process. Due to the enormous heat input from the melt particles the gas density is lowered and the gas flow is accelerated. On the other hand, another type of feed back to the gas flow results from the particles and their role as obstacles to the gas flow. Their high number concentration within the core area and their low velocities compared with the gas velocity suddenly cause a deceleration effect to the gas flow. Both types of influence will change the velocity profile as well as the turbulence structure of the gas flow and result in a dense multiphase flow of the spray cone in this region.

After having passed the core area and being already transported within the far field, the melt particles are supposed to have achieved their final size distribution, and the spray has become sufficiently dilute. Thus Phase-*Doppler*-anemometry (PDA), high speed pyrometry (HSP), high speed videometry, and patternator- as well as enthalpy- probe measurements can be used, in order to give a realistic description of the experimental conditions. These measurements show that the size distributions of the melt particles differ with material properties, with process conditions and – of course – with locations of the measuring probe. A typical PDA-result is given in Fig. 15 from [16] for different gas mass flows (M_G = 0.21 and 0.29 kg/s). A comparison of such size- and velocity- distributions, measured by PDA and HSP from an identical position in the spray cone, can be seen from Fig. 16. Different particle temperatures have been recognized, due to the overheating temperature and the thermal properties of the materials (steel Ck 35 and X20Cr13 and cupper-nickel CuNi), Fig. 17, after [17].

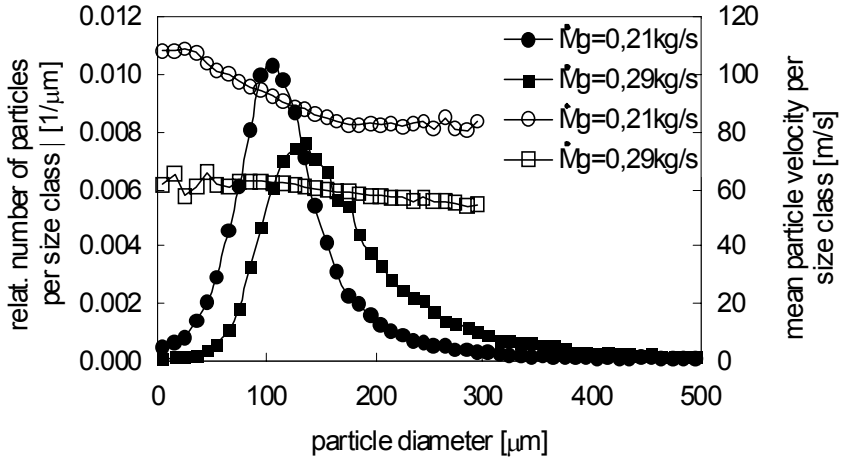

Fig. 15: PDA-results: relative particle number and (simultaneously measured) mean particle velocity per size class (i.e. particle size and velocity distribution) for different gas mass flow rates

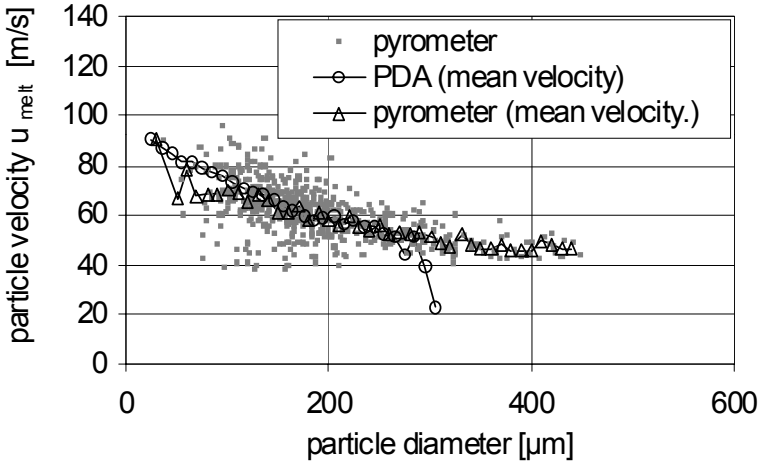

Fig. 16: HSP-results in comparison with PDA-results: particle velocity versus particle diameter

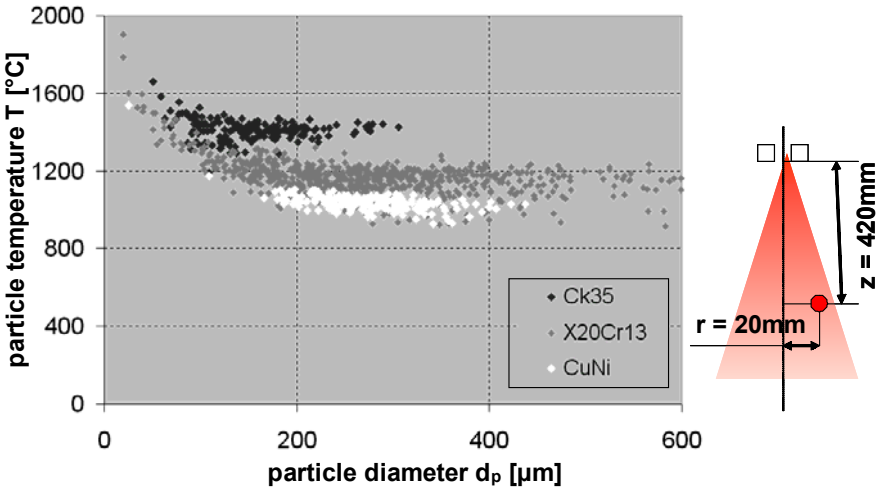

Fig. 17: HSP-results: particle temperatures versus particle diameter for different materials

3.1. Free Gas Jet and Melt Mass Flow

As has been outlined above, the pure gas flow in region **c)** forms a single free jet with the well known self similar velocity profiles (of the main axial component, see Fig. 18a from [14]), which can be described by a *Gauß*-function. Assuming a constant static pressure within this free jet, the velocity profile and the gas mass flow profile in the radial direction are of identical shape.

Hence it is not surprising to find in the far field **c)** of the spray cone (instead of the free single phase gas jet) mass flow distributions of the melt particles, similar to the radial mass flow profiles of the free gas jet, with their maximum values on the centre-line of the spray cone and with radial decrease (half value radius $r_{0.5}$) which can also be described by *Gaussian*-functions [14 and 15]. Such a typical mass flow distribution of cupper-melt particles versus radius of the spray cone, received from patternator measurements can be seen from Fig. 18b.

The free gas jet (during its impingement onto the substrate) at least is forced to flow around this extended obstacle (i.e. the substrate/deposit). This also holds for very fine melt particles which are transported by the gas stream like tracers. They follow the gas stream around the substrate/deposit because of their low inertia. As overspray-particles they will be either recirculated within the spray chamber or sucked off by the exhaust together with the waste gas. Since the amount of these overspray-powders might in some cases range of up to 40% by weight (of the melted material), strategies to raise the yield, as reported in [18], are needed.

The compaction of the partly solidified melt droplets is mainly influenced by

- the momentum of impact, while the droplets (with diameters between 1 to 300 µm) impact with (relative) individual mass differences in the range of 1 :10^7 and velocities of up to 200 m/s and
- the quantity of liquid melt within the impacting particle population as well as in the upper surface layer of the deposit surface.

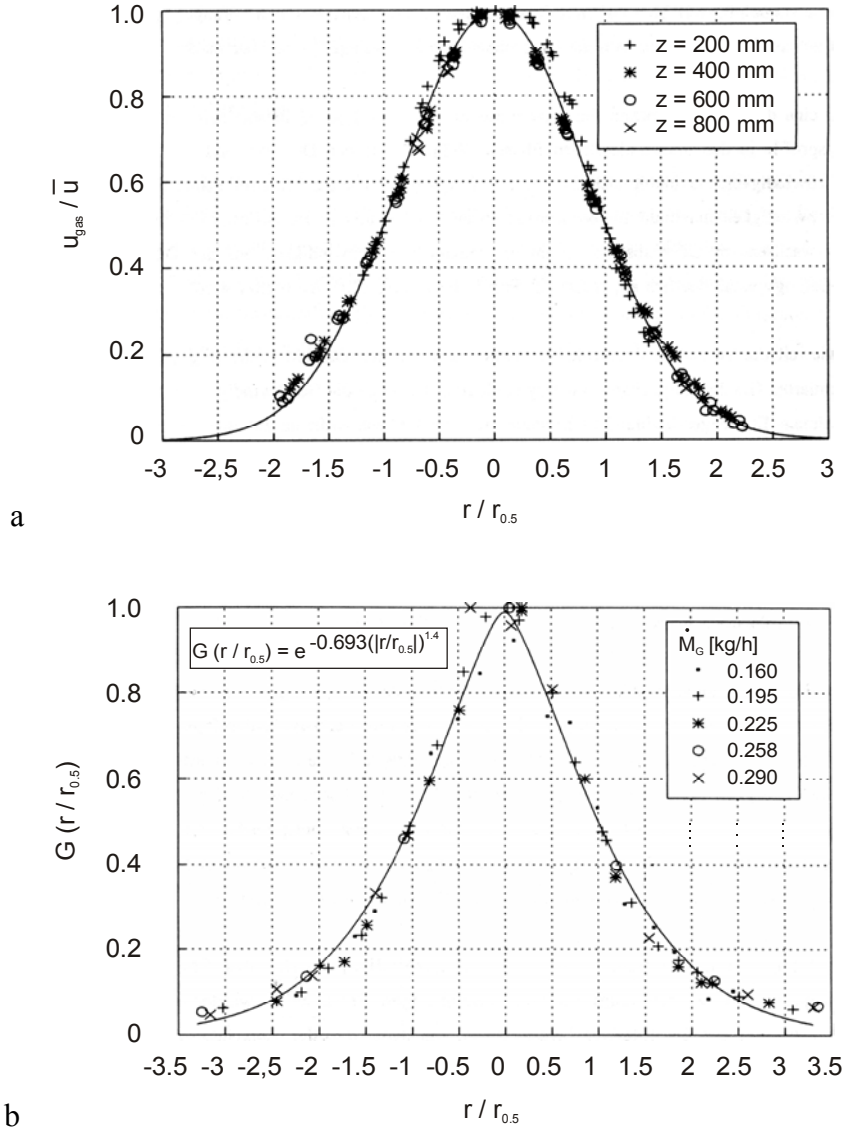

Fig. 18: a) Axial component of gas flow and b) of melt particles within the spray cone

3.2. Enthalpy-Transport

One of the main characteristics of the spray forming process is the extraction of heat from the melt particles before their compaction takes place. (This is different from the conventional ingot process, where the melt feed is completely liquid.) Already the atomization and the heat-transfer-process (within the multiphase flow of the spray cone) determine the following deposition-, solidification- and cooling- process of the growing deposit. The melt disintegration generates an enormous augmentation of the melt surface (factor 10^3 to 10^4). This is essential for the heat transfer process, with great individual differences between the smaller and the larger droplets, which can be expressed by the ratio of the individual surface area, ranging from 1 to 10^5. There result also great differences between the individual droplet accelerations (and velocities) as well as between the release of thermal energy to the gas during their flight to the substrate.

The heat extraction can be illustrated by results received from a conventional simulation model as presented in Fig.19 after [19 and 20]. The varying temperatures of the (particle free) gas and of the particles (with diameters of 10; 50; 100; 150 µm) are given versus flight distance on the centreline of the spray cone (copper particles; gas pressure 4 10^5 Pa, i.e. M_G = 0.29 kg/s). The initial melt temperature was set ΔT = 300 K higher than the melting temperature, thus the curves for the melt droplets of different diameters altogether start with the temperature 1658 K and (most of them) reach the horizontal line T_{melt} = 1358 K at different distances z from the atomization point. (This horizontal line marks the melting/solidifying temperature of the copper material.) Since the smaller particles are subject to a rapid cooling process immediately after atomization, they show a tendency of undercooling. The lowest temperature they may reach before solidification starts is given by the nucleation temperature for pure copper T = T_{melt} – 236 K. Thus, the smallest particles meet the gas temperature already at flight distances of about 10 cm. Particles of 50 µm in diameter cool down to temperatures of about 1250 K until at a distance of about 40 cm recalescence is started. Since the maximum flight distance from the atomizer to the deposit can be varied between 500 up to 800 mm, these particles as well as the larger ones are not yet completely solidified when they impact onto the deposit.

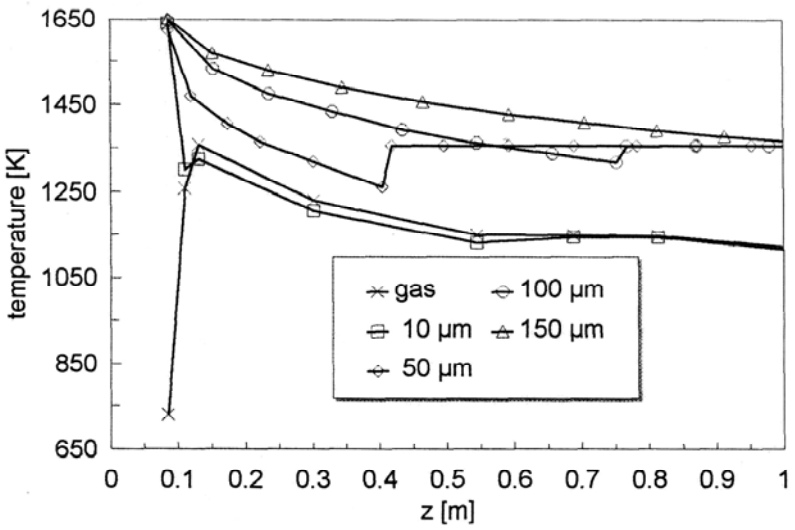

Fig. 19: Simulation results for the centre-line of the spray cone: gas and particle temperatures versus flight distance (from the atomizer)

Simulated data like these also contain the information about the momentary thermal energy of the particles at the position under focus, i.e. the information about the individual specific heat of the particles (due to their temperature) and about their latent heat (due to their fraction of still molten material). This information can be called up for each size class as well as for the entire size distribution and it can be integrated (for a fixed time) over the whole cross section of the spray cone, for instance, directly before the particle impact on the surface of the deposit takes place.

As elucidated by Fig. 20, the solid fractions f_{solid} (between 0 and 1) of the particles at some exemplary flight distances z (= 15; 50 and 68 cm downstream from the atomization point) can be given as per size class. One can see that at the distance z = 15 cm only the particles

with diameters less than 10 µm are already completely solidified whereas those with diameters larger than 50 µm are completely molten. For the distance of 50 cm the field has spread significantly. At least for a distance of 68 cm (this could be, for instance, the distance where the impact onto the deposit takes place) particles with diameters of about 8o µm completely cover the field between $0 < f_{solid} < 1$, those with diameters > 90 µm contain a significant portion of liquid, those with diameters >200 µm are still completely liquid, and those with diameters < 30 µm already completely solid.

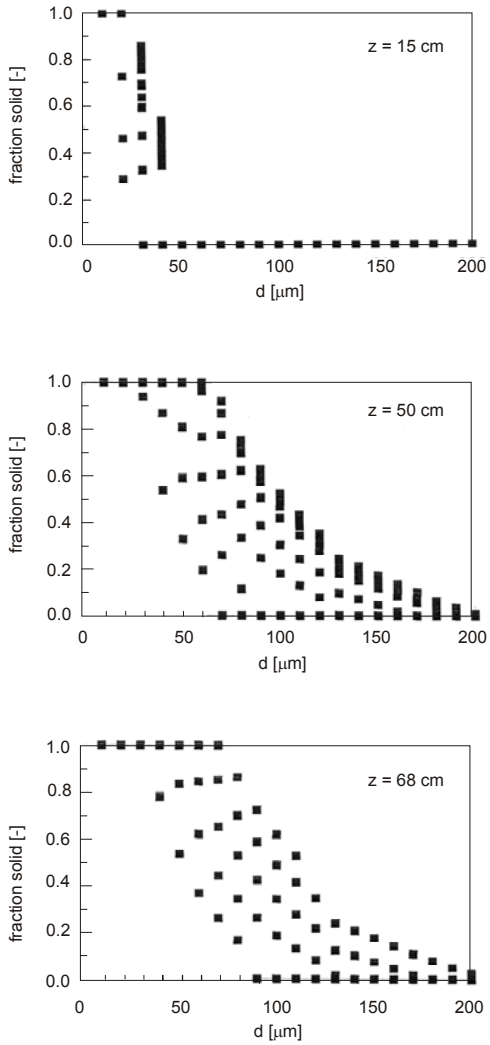

Fig. 20: Fraction of solidified particles at different distances from the atomizer

In order to prove these computational results by experimental data, HSP-measurements have been executed (results of this type have already been shown in Fig. 16 and 17) as well as enthalpy-probe-measurements, collecting particles from the spray cone and checking their enthalpy and mass flux at different positions within the spray cone. Typical results, exemplary given in Fig. 21 a and b from [21], show the dependency of the local specific enthalpy of the collected particles from

i) distances z from the nozzles on the centreline of the spray cone (of steel particles, Ck 35) for different overheating temperatures ΔT = 100 and 200 K,

ii) distances r from the centreline (of copper particles) for different over-all melt mass flows (M_L = 0.27 and 0.19 kg/s) and a constant overheating temperature ΔT = 200 K.

In both diagrams the over-all gas mass flow rate is given as M_G. Though from these measurements no answer can be given about the individual particle temperature (as has been received from the HSP) or about the individual particle enthalpy, the computed and measured local or integral enthalpy of the particle collective just before impact is of same importance.

a

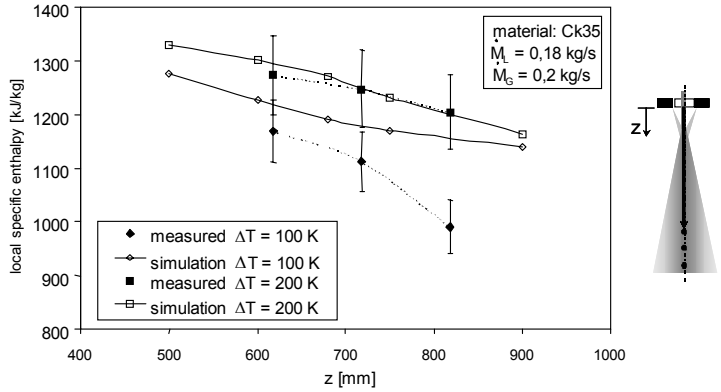

b

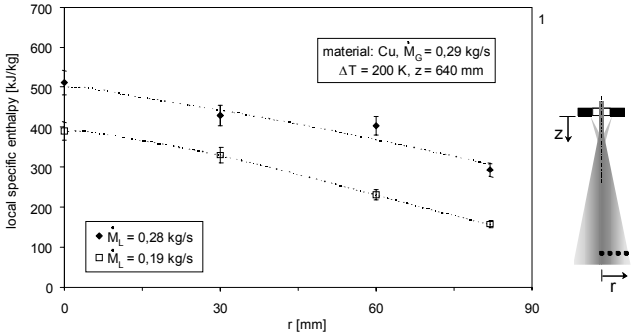

Fig. 21: Local specific enthalpy of collected particles: a) steel, versus flight distance for various overheating temperatures, b) copper versus radius of the spray cone for different melt mass flows

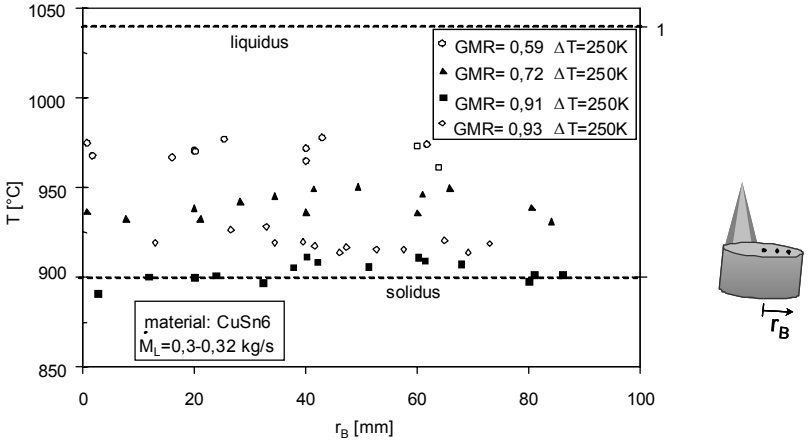

Fig. 22: Measured local surface temperatures versus billet radius for different GMR

For instance, for small groups of particles it has been measured such enthalpy and mass fluxes at various positions within the spray cone (also just in front of the upper surface of the deposit) as can be seen from Fig. 21 .

This enthalpy input into the mixing layer is of main interest for the solidification process. Therefore as a further reference method a pyrometer has been used, from which one gets information about the surface temperature of the mixing layer. Typical results – as have been received, for instance, from the upper surface of a cylindrical deposit (copper-tin, CuSn6) – are given in Fig. 22 from [21] showing temperatures (versus billet radius r_B) ranging between liquidus and solidus, depending on the mass flow ratio of gas to melt (GMR).

From chapter 4.1 and 4.2 it follows that mainly the parameters of the melt particle size distribution (in a first approximation: the mass median diameter $d_{50.3}$) become important for the transport process of mass, momentum and enthalpy. Therefore it is essential to receive this information from the particles as "in-process" measurements (in-line and on-line), if one intends to model and control the entire spray forming process and to derive strategies for directly influencing the resulting material properties of the growing deposit.

3.3. Powder Addition

In addition to the high alloying flexibility of the basic spray forming process, there exists the possibility (i.e. a further important potential) to introduce additional (metallic or ceramic) powder materials to the spray cone. These materials, for instance, may not be miscible with the basic melt, but can be embedded within the matrix of the deposit material.

Many applications require an uniform distribution of the powder particles within the deposit and also demand that the above mentioned advantages of the process will not be given up. So efforts to generate promising material properties of the metal matrix composites are concentrated on the distribution of the powder feed. (If on the other hand deposits have to be generated, showing definite gradients of the materials properties, the powder has to be added by different methods and without the demand of a well distribution within the spray cone and in the deposit.)

The powder is added pneumatically to the spray cone under stationary conditions. This also holds for the mass flow of the melt droplets and of the atomization gas. Only stationary mass flows can guarantee a constant mixing ratio of melt and added powder during the entire process, hence one has to introduce the powder to such an extent, that it has a real chance to reach this well distribution at first within the multiphase flow of the spray cone on its way to the deposit. Locations close to the primary gas nozzle turned out to be the optimal positions for the powder introduction.

Introducing the powder feed close to the primary gas nozzles into the (not jet fully developed) free (gas) jet, one can measure further downstream profiles of the local mass flow rate of the additional powder as given in Fig. 23. These radial profiles differ with material properties (Cu, Fe, SiC, Al) and are in principle similar to those measured for the melt particles. For the powder particles an isokinetic probe has been used – for the melt particles a patternator; both probes had positions downstream in the free jet and the spray cone respectively [22]. Because of the minor amount of powder feed compared with that of the melt (powder

to melt mass flow ratio PMR), the results lead to significant lower radial profiles, as given in Fig. 24. Thus, one is allowed to suppose for this location of powder introduction that the spreading powder within the spray cone follows the same laws of mass- and momentum-transfer as the melt particles do and that – if the atomization works – both, the powder and the melt particles, are well distributed .

The finer the powder particles and the lower their density, the higher is their tendency to follow the gas flow, like tracer particles do. This means that not only the gas flow stops its straight movement just in front of the substrate/deposit, now being forced to flow around this obstacle, but this also holds for the fine powder particles. While denser and larger particles – due to their higher inertia – do not follow this sudden redirection and impinge – as directed – on the deposit (where they are embedded together with the melt particles), there will be an important part of the fine powder transported into the overspray. This means that there will be found a smaller amount of (for instance) a very fine graphite powder (with a density of only 2.26 g/cm^3) in the deposit compared with a coarser and denser cupper-powder, though there have been added identical quantities. The deficits in the deposit lead to additional contributions to the overspray and will change the balances in the cyclones and filters.

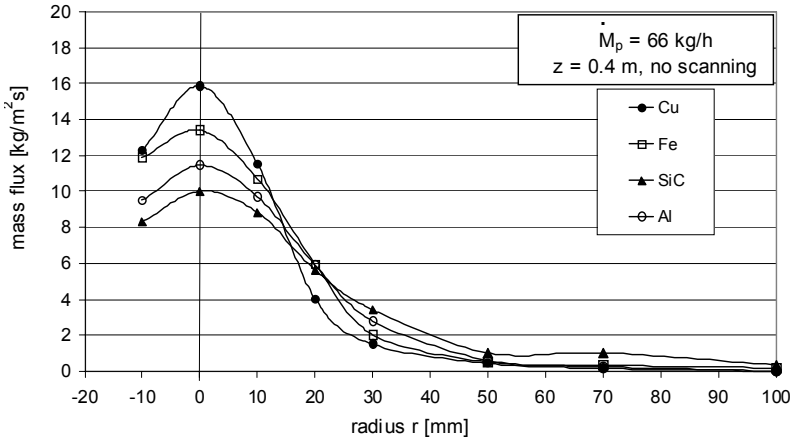

Fig. 23: Mass flux of different powders versus radius of gas jet

If finer and less dense powders are added to the spray one can recognize an increase of the powder concentration within the deposit versus process duration. This is caused by the fact that the spray cone, which exhibits a somewhat smaller radial extent than the free gas jet, entrains a considerable amount of recirculating gas (containing dust). This dust consists of very fine overspray particles and of course of those powder particles which have been transported into the overspray. The recirculating gas will be saturated by the powder after a measurable time, after which its concentration remains stationary. Until this moment the powder saturation of the entire gas atmosphere of the recipient is also rising, thus, leading to a likewise rising powder concentration within the spray and therewith in the material of the deposit (increase of concentration with height and diameter of the billet).

In the vicinity of the atomizer not only melt disintegration and acceleration of melt and powder particles take place during their movement to the deposit, but also particle collisions due

to the dense flow in this region. As far as the melt particles are still liquid and the surface tension between powder and melt allows an adhesion (and moistening) of the powder particles these collisions lead to surface coating- (or wetting-) effects of a considerable amount of powder.

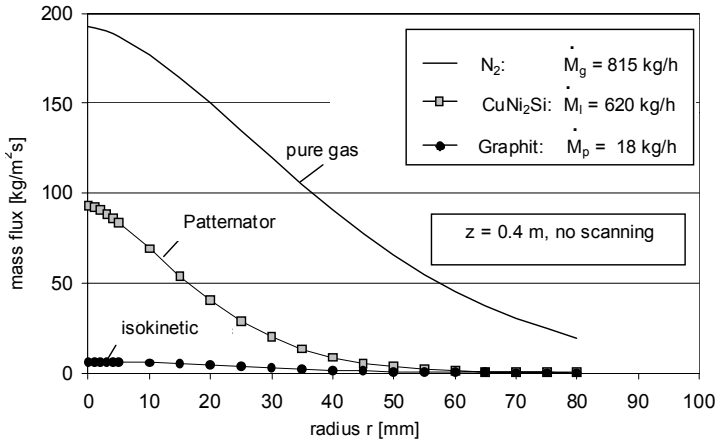

Fig. 24: Comparison of radial distributions of gas mass flow, melt mass flow and powder mass flow, measured by different methods

This results in an easier embedding. Samples taken from the overspray show that for instance steel powders are wetted (coated) fairly good by the matrix material copper, see Fig. 25 from [23]. On the other hand wetting (coating) of graphite powder particles by the same matrix material seems to fail, which explains the enrichment of these particles at the grain boundaries and at the borders of splashed droplets within the deposit, if the process has been operated too cold. One may assume that these results confirm the role of the surface tension of those materials.

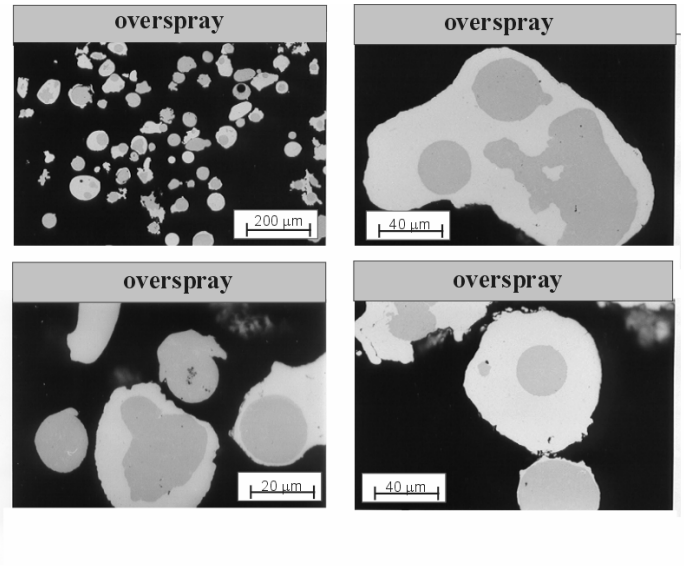

Fig. 25: Particles collected from the overspray showing wetted steel particles (with copper-tin-melt)

Nevertheless, one has also to focus on the momentum of these collision partners. Due to their geometry, particles of same size show a lower probability of collision than a combination of very small particles on the one side and large particles on the other. But in combination with their density (lower density of the small particles) and in accordance with the differences of their velocity compared with the gas flow in their vicinity, there results a movement of the small particle around the large obstacle, lowering the number of collisions significantly. This phenomenon, for instance, can be described by means of the *Stokes*-number (discussed in detail in [24])

The process opens a wide choice of materials processing and especially of influencing the material properties of the deposit by adding powders to the main stream of metal melt droplets. Since the powder particles will be compacted together with the melt particles, forming a deposit, both particulates will metallurgically react and generate a metal matrix with new properties. The powders may consist of various materials with specifications differing from those of the matrix material (for instance not miscible in the liquid melt state) or consist of the same material as the matrix, i.e. of overspray. (The reinjection of overspray to the spray cone may raise the yield of the product significantly.)

4. Deposition and Compaction Process

The solidification of the impacted material on the deposit comes to pace within a semi-solid zone at the upper surface layer (the so called mixing layer), starting from a great number of fine and already solidified particles. Since the residual quantity of liquid melt within the semi-solid layer is small, only very short distances between the solid particles appear for the final solidification. These short distances prevent segregation and give rise to very fine grains in the microstructure. Also shrinking of the solidifying material within the mixing layer is low because the solidification process, and therefore the volume reduction, has started already during the flight of the particles in the spray cone.

Provided that the conditions of atomization and multiphase flow situation in the spray cone remain stationary, one may assume for a cylindrical deposit (a billet, with its diameter in the range of its height) also a stationary thermal situation within the semisolid mixing layer at its top. For a first approximation influences due to heat losses at the billet-shoulder and at the cylinder jacket are neglected. One furthermore may assume a thin flat zone of nearly constant height S_M versus radius just below the upper billet surface, where the particle stream from above continuously impacts on to the deposit.
For this model are presumed three different parallel zones, as sketched in Fig. 26a) from [25]:

α) a thin crust or coating film (for instance of extremely fine, already solidified particles) being in contact and heat exchange with the nitrogen atmosphere of the spray cone,

β) a suspension bed (with still a sufficient entire amount of melt) of moderate thickness and high viscosity (giving the name for the complete mushy zone: mixing layer) and

γ) a layer at the bottom of zone β), where final solidification takes place (thus leading from a solid fraction $\Gamma_{solid} < 1$ to the value of 1)[1].

These three zones of the cylindrical deposit are illustrated in Fig. 26 with various fractions of solid and liquid material differing mainly with the distance from the upper surface but remaining constant versus radius.

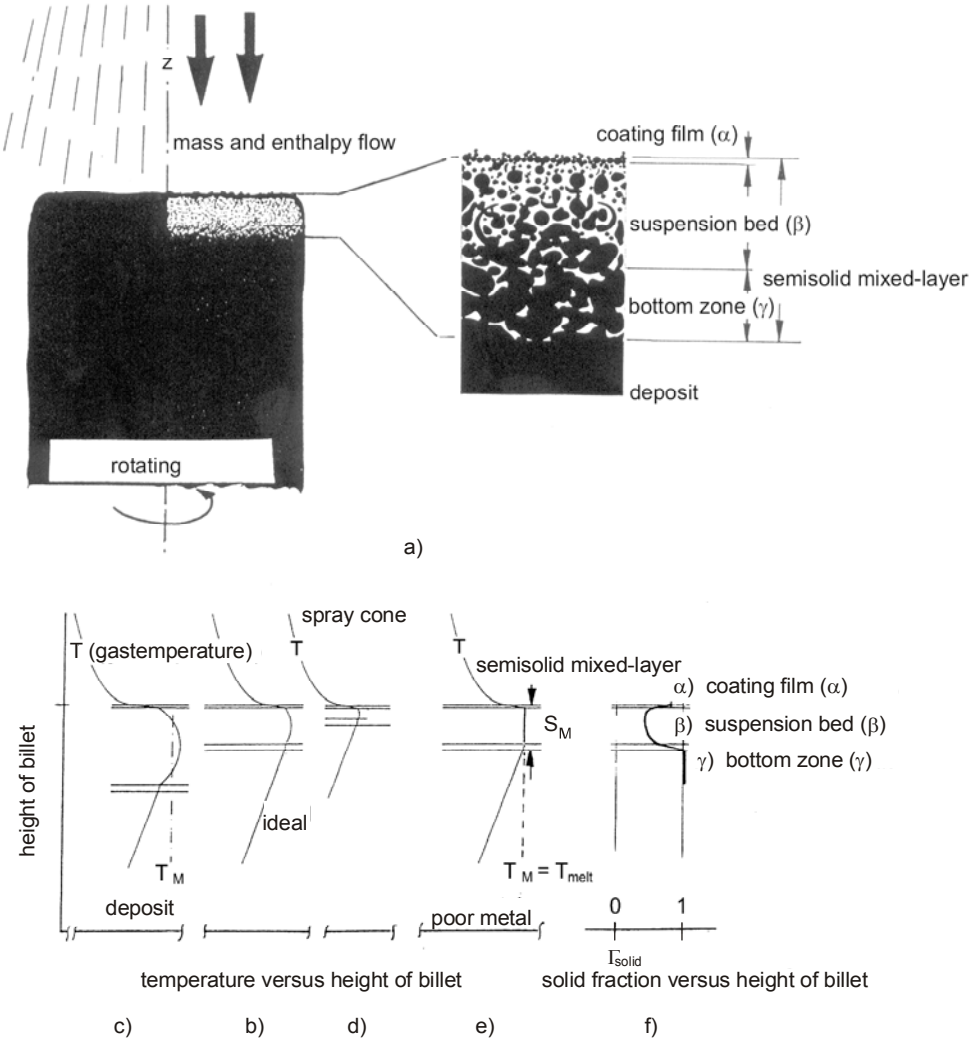

Fig. 26: Model of the mixing-layer: b) ideal status; c) status with higher amount and d) status with lower amount of enthalpy; e) and f) status of a pure metal

Depending on the enthalpy input from the spray cone these three zones: (α) + (β) + (γ) act as a buffer with their common thickness S_M, their temperature T_M, and the fraction of solid material Γ_{solid} as sketched in Fig. 26f). If there is (hypothetically) a sudden and moderate increase or decrease of the enthalpy input from the melt particles, the thickness S_M will change from an ideal status b) to that sketched in section c) or that in section d), after having returned to a new stationary situation.

[1]) The solid fraction Γ_{solid} within the mixing layer may be, – but is not necessaryly identical with that of the particle population f_{solid}.

In case of a pure metal (no alloy) – as sketched in Fig. 26e) and f) - the temperature of the semisolid mixing layer is fixed at the constant solidification (or melting) temperature T_{melt} and the only variables are now the layer thickness S_M and the quantity of solid material Γ_{solid} (between 0 and 1) which are able to react on variations of the enthalpy input.

The dispersed particles in the spray cone exhibit a cooling and most of them a solidification process within a split of a second. This leads – as soon as the particles solidify – to a dendritic structure with very short dendritic arm spacings. These short distances cause short diffusion times (of only seconds up to a few minutes) for the following equalizing diffusion processes, taking place after impact in the semisolid mixing layer of the deposit. The temperature level between liquidus and solidus and the high concentrations of already solidified particles within the mushy zone (in the semisolid mixing layer) lead to an unidirectional crystallization process over very short distances between the solid particles. Together with the controlled cooling process of the preform this explains the fine equiaxed grain structure and the macroscopic uniformity of alloying elements within the microstructure and finally the chemical and morphological homogeneity of the sprayed material. The dynamics of these process steps and the special buffer function of the mixing layer during process parameter fluctuations influence the quality of the spray formed material.

During the spray forming process (without adding powder) the convective heat transfer from the melt to the gas is governed by the tremendous enlargement of the particle surface (after atomization). Introducing additional powder to the gas stream leads to an increase of the heat capacity of the gas/powder mixture. This means, a) that the melt is able to transfer an extended amount of heat to the gas/powder mixture along its way to the deposit and b) that on the other hand this gas/powder mixture will not heat up along the same distance as much as the pure gas does. The result is a cooler mixing layer compared with that, resulting from the powder free spray forming process.

A more differentiated enthalpy balance of the spray forming process, including now the addition of powder, explains not only the observation of a cooler mixing layer but also the reduction of grain size: The additional powder particles, embedded in the mixing layer, have a lower temperature than the other metal particles in their immediate vicinity which are still liquid and/or (partly) solidified or have temperatures between liquidus and solidus. So the powder particles are acting as heat sinks upon their neighbourhood in the mixing layer and accelerate the total solidification and/or the cooling process. This explains the fact, that within the deposit the grain size of (for instance) a CuNi2.4Si0.6 material has been reduced after addition of graphite powder to the spray cone (in comparison with the powder free process), see Fig. 27 from [26].

One may assume that there are sufficient or more nuclei in the mixing layer for the grain growth process – which results from the very fine unavoidable overspray powder, its permanent entrainment into the spray cone via the recirculating gas stream and its embedding into the deposit. Grain growth in competition with nucleation begins with sufficiently high temperatures. The result, the grain size, is proportional to the temperature and the duration on this temperature level. In the mixing layer both preconditions (the high temperature and the time duration on this level) are principally fulfilled, but also limited by the cooling process. By embedding the cold powder particles into the mixing layer this limitation of grain growth will become more critical, since the duration for the grain growth and the temperature level will be reduced. Furthermore the diffusion processes, which are necessary for the grain

growth, will be hindered by the grain boundaries respectively by different phases and/or materials.

By embedding additional powder particles of different materials in the mixing layer, there result grain boundaries with an increased level of hindering the diffusion processes. This has been figured out after fine graphite-powders with growing concentrations have been added to a copper-matrix. For this combination the grain size has been reduced significantly from 350 to 35 µm (as measured in the deposit) and can be seen in Fig. 27.

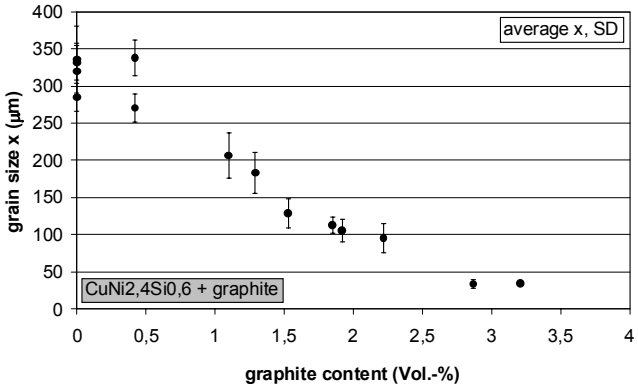

Fig. 27: Grain size variation of the copper based alloy with concentration of added graphite

On the other hand – depending on the decrease of heat content in the mixing layer with increasing addition of powder and thus referred to the lower amount of residual liquid melt within the mixing layer – the possibility of growing porosity arises. A decrease of liquid melt means a reduction of filling up pores in statu nascendi. This can be seen from Fig. 28, which shows an increase of porosity with growing concentrations of powder, and this has been quantified by the diagram of Fig. 29. In order to hold the porosity on a low tolerable

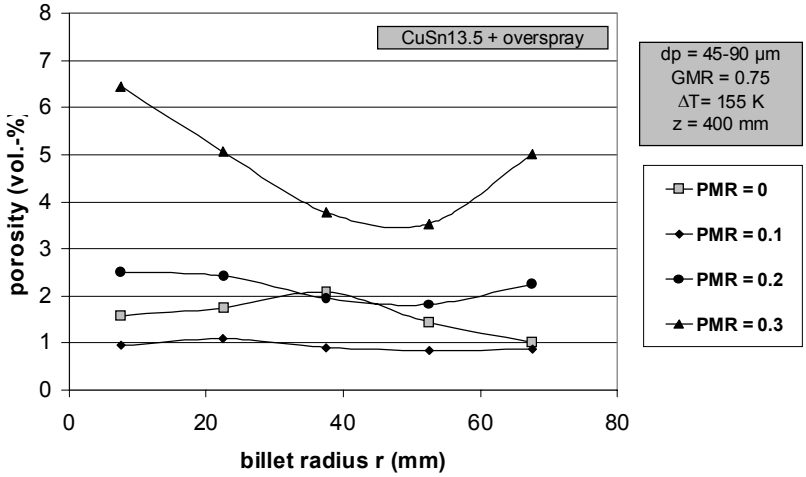

Fig. 28: Radial porosity profiles of copper based alloy with various PMR of the added overspray powders

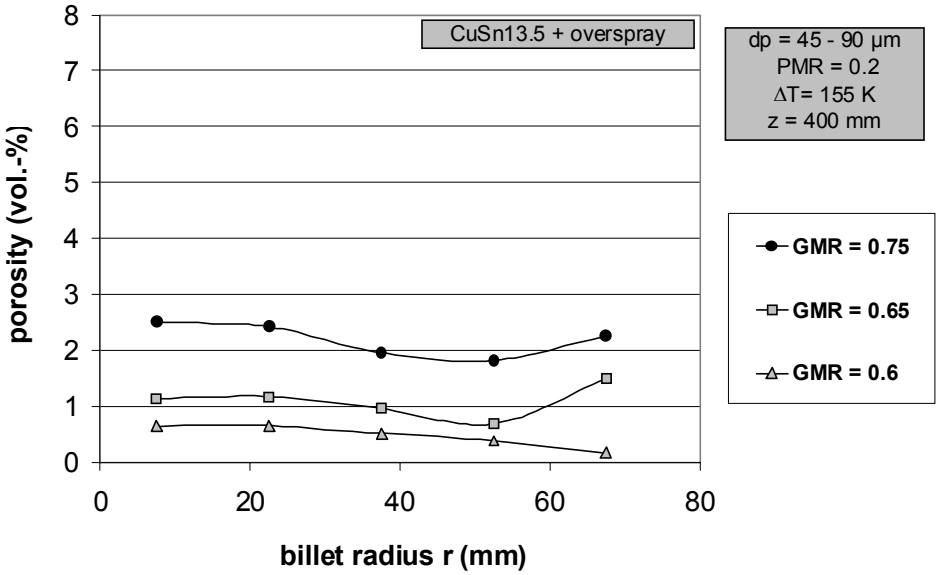

Fig. 29: Radial porosity profiles of copper based alloy with various GMR

level, one has to increase the overheat of the melt, thus compensating the higher heat losses resulting from the augmentation of the powder feed. This is lifting up the amount of residual melt in the mixing layer. Nevertheless the advance is a grain fining effect due to the enlarged amount of boundaries (of the different material) of the powder particles.

5. Process Control

One of the most important process parameters in spray forming is the size distribution of the melt droplets. As already pointed out, the melt particles are supposed to have achieved their final size distribution after passing the core area and being already transported in the far field of the spray cone, i.e. at a distance of about 150 mm downstream the atomization point. Here the secondary break up of droplets and the successive droplet break up after collision processes in the dense flow region are assumed to have come to an end. Measurements by different methods have been taken from this position and from positions further downstream, in order to analyse the multiphase flow conditions within the spray cone under various parameter settings [27 to 29]. After adapting the phase-Doppler-anemometry to the rough process conditions of the spray chamber, this technique has been upgraded, in order to develop a control system based on on-line and in-line particle size and simultaneously particle velocity measurements. (Details of these developments are discussed in [16 and 27]. The control loop and the PDA set-up are sketched in Fig. 30 and 31.) The purpose of these investigations was to develop a control system which allows a fast variation of the atomization gas pressure if, for instance, melt flow fluctuations demand of a correction of the GMR.

As can be seen from Fig 32, the time needed for an adjustment of the atomization gas pressure (in order to receive the required mean diameter of the melt particles) is less than 50 seconds. This time duration depends on the process conditions because there have to be collected statistical sufficient counts in order to receive a representative value for the mean particle size. In Fig. 32 as a mean diameter has been used the 50%-value of the PDA number size distribution after 10^3 counts.

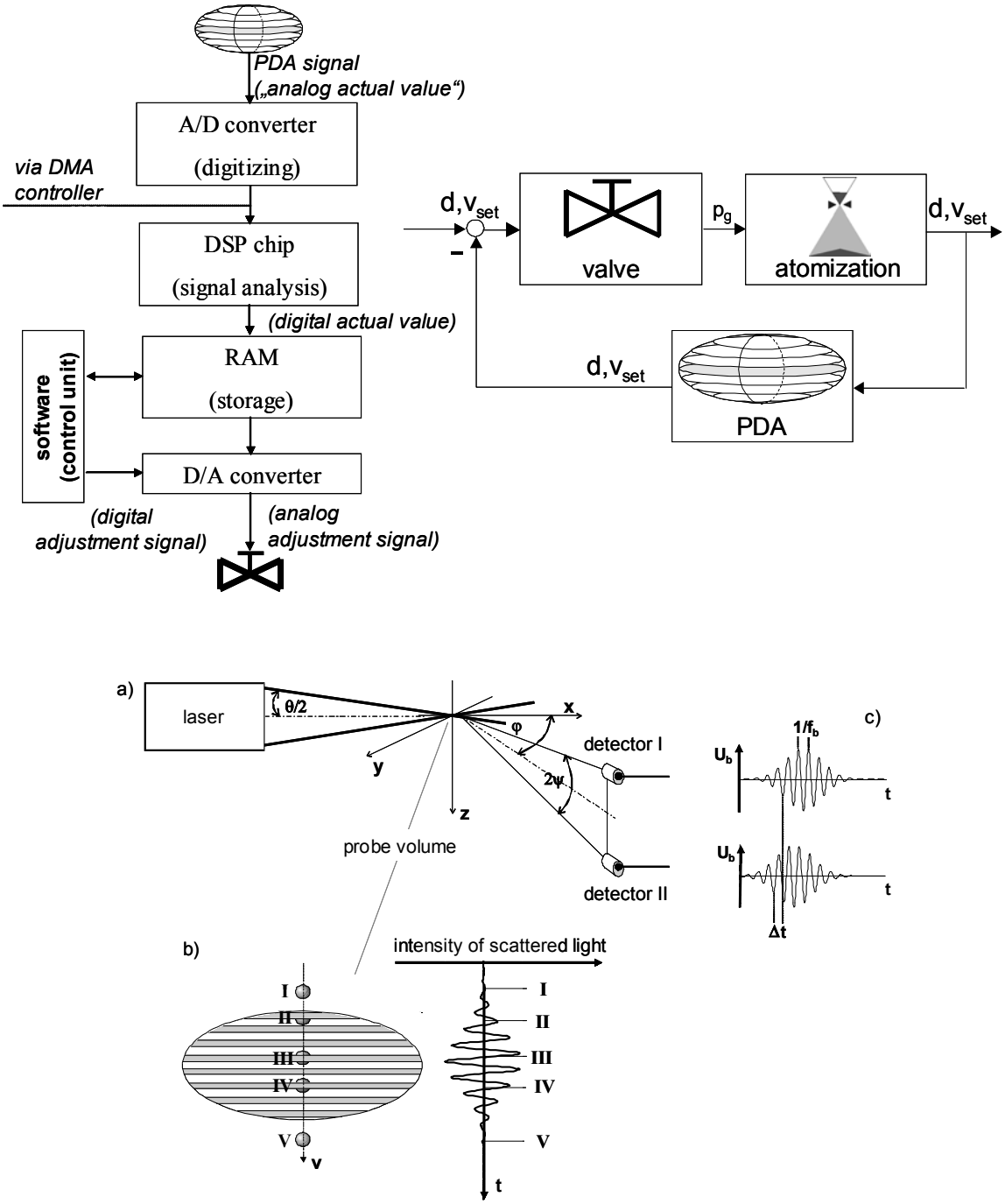

Fig. 30 and 31: Control unit and PDA-set-up for controlling the particle size- and velocity-distribution by adjusting the atomization gas pressure

Typical fluctuations during the process arise from oxidation phenomena at the melt outlet, which may reduce the melt flow. Other problems arise if growing mass flows of powder have to be added in order to generate products with gradiented material properties. Here the GMR has to be adapted (increased) to the variation (decrease) of the enthalpy input into the mixing layer.

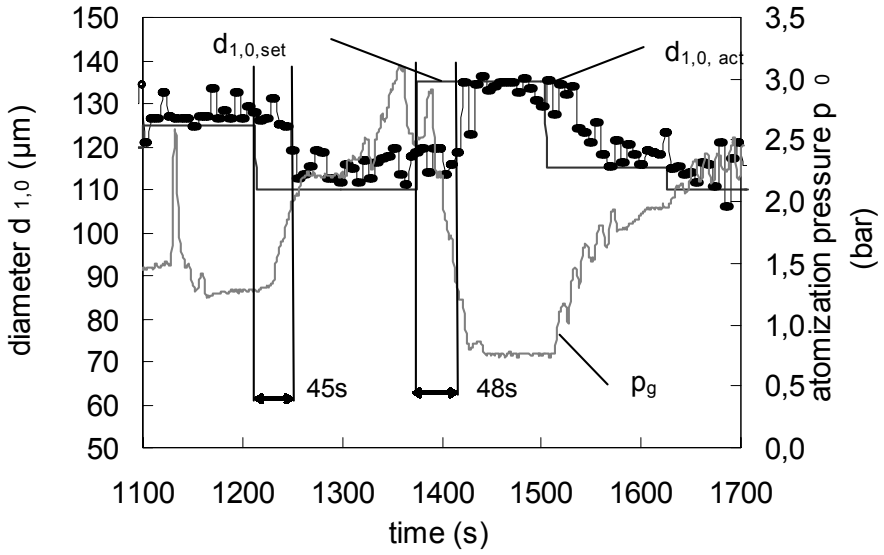

Fig. 32: Measured mean particle diameter and adjusted atomization gas pressure: time between adjustment and result

6. Summary

As has been outlined, the main unit operations:

- the twin fluid gas atomization of (various) melts,
- the mass-, momentum- and enthalpy-transport (rapid cooling of the droplets) of the melt particles within the multiphase flow of the spray cone, directed onto the deposit, as well as
- the deposition, compaction and solidification of the melt particles (together with the added powder particles) within the mixing layer of the deposit

are not only consecutive but also conditional steps of the spray forming process and its material properties creating function.

The purpose of our investigations was to understand and describe the atomization process as a base for modelling (and control) of the overall disintegration process and to derive strategies and possibilities for directly influencing the resulting spray properties (and in consequence the material properties of the deposit) of the atomization process. In correspondence with experiments the numerical simulation of the gas flow situation in the vicinity of the individual gas nozzles and their common influence on the melt jet perturbation led to improved atomizer design and thereby higher efficiency of the disintegration process (smaller droplets, lower span and reduced gas consumption).

Since in the atomization stage the mass flux distribution and enthalpy density distribution in the spray are determined (resulting from the different sizes of droplets and particles and their short thermal histories during their flight within the spray cone from the atomization zone to the impingement onto the deposit surface), the strategy of process control was, to measure the main parameters of the atomization result in-line and on-line, i.e. the size distribution of

the melt particles and simultaneously their velocity distribution, and to base the adjustment of the atomization gas pressure on these in-process measurements.

The analysis of the multiphase flow situation in the spray cone helped to explain the transport mechanism of the added powders for the generation of metal matrix composites and to optimise the powder injection.

7. Acknowledgement

The author would like to thank the Deutsche Forschungsgemeinschaft (DFG) for the financial support under the SFB 372.

8. References

[1] A.R.E. Singer: Recent Developments and Opportunities in Spray Forming; Sprühkompaktieren- Kolloquium, Band 1, ISBN3-88722-363-2, Universität Bremen (1996) S. 123 -139

[2] A.R.E. Singer: The Principles of Spray Rolling of Materials; Met. Mater., Vol. 4, 1970, pp. 246-250

[3] A.G. Leatham; R.G. Brooks; J.S. Coombs; A.J.W. Ogilvy: The Past, Present and Future Developments of the Osprey Preform Process, Proc. First Int. Conference on Spray Forming, Osprey Metals Ltd., Neath UK (1991) Section 1, Paper1

[4] R.G. Brooks; J.S. Coombs; A.G. Leatham; H. Mort; C. Moore: The Structures and Properties of Some Spray Forged Aerospace Materials, Modern Development in Powder Metallurgy, Vol. 11, 1977, pp.1-12

[5] Sonderforschungsbereich Sprühkompaktieren 372: http://sfb372.iwt.uni-bremen.de

[6] N. Dombrowski; W.R. Johns: Chem. Eng. Sci. 18 (1963) pp. 203-214

[7] E. Klar; J.W. Fresko: Powder Metallurgy Handbook, Vol. 7, nineth. ed. American Society for Metals, Material Park, OH, 1984

[8] U. Fritsching: Spraysimulation; ISBN 3-8265-8179-2, Shaker Verlag, 2001

[9] H. Lohner: Zerstäuben von Mineralschmelzen mit Heißgas; Dissertation, Univ. Bremen 2002; Fortschritt-Berichte VDI, Reihe 3 Verfahrenstechnik Nr. 765, VDI-Verlag Düsseldorf

[10] U. Heck: Zur Zerstäubung in Freifalldüsen; Dissertation, Univ. Bremen 1998; Fortschritt-Berichte VDI, Reihe 7 Strömungstechnik Nr. 348, VDI-Verlag Düsseldorf

[11] H. Lohner; C. Czisch; P. Schreckenberg; U. Fritsching; K. Bauckhage: Atomization of Viscous Melts; to be published in Atomization and Sprays

[12]- S. Markus; U. Fritsching; K. Bauckhage: Jet Break UP of Liquid Metal in Twin Fluid Atomisation, Mat.Sci. a. Engng, A 326 (2002) pp. 122-133

[13] S. Markus; U. Fritsching: Instability Processes in Melt Atomization, Proc. Of the 2002 Powder Metallurgical and Particulate Materials, Orlando, June 16-21; 2002, pp. 3/137– 3/149

[14] V. Uhlenwinkel: Zum Ausbreitungsverhalten der Partikeln bei der Sprühkompaktierung von Metallschmelzen; Dissertation Univ. Bremen 1992; Fortschritt-Berichte VDI, Reihe 3 Verfahrenstechnik Nr. 300, VDI-Verlag Düsseldorf

[15] C. Kramer: Die Kompaktierungsrate beim Sprühkompaktieren von Gaußförmigen Deposits, Dissertation, Univ. Bremen, 1997

[16] J. Ziesenis: Weiterentwicklung der PDA-Meßtechnik zur on-line Prozesskontrolle beim Sprühkompaktieren; Dissertation, Univ. Bremen, 2002

[17] M. Krauss; D. Bergmann; U. Fritsching; K. Bauckhage: In-situ Particle Temperature, Velocity and Size Measurements in the Spray Forming Process; Materials Science and Engineering A 326 (2002) pp. 154-

[18] V. Uhlenwinkel; A. Schneider; Th. Wriedt; H. Harig; K. Bauckhage: Effect of Particle Injection During Spray Forming of Cu-Sn Billets; Proc. of the Int. Conf. on Powder Metallurgy & Particulate Materials (PM2TEC), Orlando, 2002

[19] D. Bergmann: Modellierung des Sprühkompaktierprozesses für Kupfer- und Stahlwerkstoffe; Dissertation, Univ. Bremen, 2000

[20] D. Bergmann; U. Fritsching; K. Bauckhage: Thermische Simulation des Sprühkompaktierprozesses; HTM 56 (2001) 2 S.110 - 119

[21] M. Buchholz: Untersuchung des Kompaktierverhaltens an sprühkompaktierten Bolzen; Dissertation, Univ. Bremen, 2002

[22] A. Schneider; R. Klein; V. Uhlenwinkel; H. Henein: Investigation of Local Particle Mass Flux in a Jet Stream with an Isokinetic Probe; Symposium Spray Forming , SFB 372, Vol. 6 , pp. 129-148, University Bremen 2002

[23] A. Schneider; V. Uhlenwinkel; Th. Wriedt; H. Harig; K. Bauckhage: Study on the Distribution of Al_2O_3- and Graphite- Particles in Spray formed Copper ($CuNi_2Si$); Proc. of the Int. Conf. on Spray Deposition and Melt Atomization (SDMA) Bremen, 2000

[24] K. Bauckhage; A. Schneider: Spray Forming Technology for Powder Metallurgy Materials and Components; to be published in Part. Part. Charact.

[25] K. Bauckhage: Das Sprühkompaktieren – ein neuartiger Urformprozeß; HTM 57 (2002) 4, S. 224-233

[26] A. Schneider; V. Uhlenwinkel; Th. Wriedt; H. Harig; K. Bauckhage: Sprayforming of MMC – Study on the Particle Distribution in $CuNi_2Si$ billets with Graphite; Proc. of the Int. Conf. on Powder Metallurgy & Particulte Materials (PM2TEC), New Orleans , 2001

[27] J.Tillwick: Einsatz der PDA-Meßtechnik zur Charakterisierung des Sprühprozesses bei der Zerstäubung von Metallschmelzen; Dissertation, Univ. Bremen, 2000

[28] J. Ziesenis; K. Bauckhage: Monitoring the Spray Forming Process; Symposium Spray Forming; SFB 372, Vol. 6, pp. 111-128, University Bremen 2002

[29] J. Ziesenis; K. Bauckhage: Absorption and Scattering of Light by Highly Concentrated Two-Phase Flows; Part. Part. Charact. (2002) pp. 195-202